LAGRANGEAN ACCELERATION MEASUREMENT IN FULLY DEVELOPED TURBULENCE

Yoshiyuki Tsuji
Department of Energy Engineering and Science,
Nagoya University
Chikusa-ku, Nagoya city, 464-8603, Japan
c42406a@nucc.cc.nagoya-u.ac.jp

ABSTRACT

Pressure is a fundamental quantity contained in the dynamical equation of fluid motion. In a usual notation, pressure relates to the acceleration vector, which is decomposed into the contributions from the pressure gradient and viscous force while the fluid density is constant. Although the acceleration may be important and basic representation of fluid motion, and Lagrangian acceleration is the core of the kinematic theory of turbulent dispersion, its direct measurement was very difficult. In this paper, we evaluate the acceleration by means of pressure fluctuation because, at large Reynolds numbers, the viscous contribution to the acceleration can be ignored. Accordingly, the acceleration is evaluated as the pressure gradient. Measured data are compared with direct numerical simulation. And the shear effect on the acclera-tion is discussed.

INTRODUCTION

The motion of fluid particles as they are pushed along the trajectories by fluctuating pressure gradient is fundamental to transport and mixing in turbulence. It is essential in cloud formation, atmospheric transport, chemical reaction process, and in combustion system. In principle, fluid particle trajectories are easily measured by seeding a turbulent flow with small tracer particles and following their motions with an imaging system. But, in practice, this can be a very challenging task because we must fully resolve particle motions which take place on the order of Kolmogorov time scale. This kind of measurements was achieved (La Porta et al., 2001) with using a specially designed particle tracking system in high energy physics and PIV system (Ayyalasomayajula et al., 2006).

In a usual notation, acceleration vector is given by N.S. equation as follows; $\mathbf{a} = D\mathbf{u}/Dt = -\nabla(p/\rho) + \nu\nabla^2\mathbf{u}$. This means that acceleration is decomposed into the contribution from pressure gradient and viscous force while the fluid density is constant. In a fully developed turbulence, the viscous damping term is small compared with the pressure gradient term, therefore, the acceleration is closely related to the pressure gradient. In this study, lagrangian acceleration is evaluated by measuring the instantaneous pressure fluctuations.

We have developed the accurate pressure measurement technique. As it will be mentioned in the later section, pressure probe consists of a standard Pito-static tube and 1/8 inch condenser microphone, and several points are taken into account for accurate measurements. For instance, HR (Helmholz resonance) and standing waves in static tube should be removed. Flow attach angle and special resolution are another important factors. Using this technique, we have measured so far the pressure intensity in the cylinder wake, square jet, and boundary layer. The spectral shape, the correlation between wall pressure and pressure in the boundary layer, the velocity pressure correlation, and probability density function were studied. They were carefully compared with DNS (Tsuji and Ishihara, 2003). These results encourage us to evaluate the acceleration by means of pressure gradient measurements.

Pressure gradient measurement was performed by using two pressure probes. The pressure difference measured at a distance Δy(or Δx) becomes pressure gradient dp/dy(or dp/dx) as far as Δy (or Δx) is sufficiently small. Calculating the statistics, such as probability density function and spectrum, they are compared with previous results. Also the shear effect on the acceleration is discussed.

EXPERIMENTAL CONDITION

Driving mixing layer

The region of primary examination in this study is the centerline of the driving mixing layer generated by a square jet from the jet exit to six diameters downstream (see Fig. 1). In this region flow reversals are unlikely and large yaw angles by the flow are infrequent. Because both mean shear and turbulent intensity are large, it provides large pressure fluctuations which can be accurately measured. The nozzle exit size is 700×350mm. The velocity sensors and pressure sensors were mounted on the traversing supports which provided full three-dimensional positioning with separations.

Self-preservation of the shear layer profile is demonstrated for the mean velocity and for the r.m.s. value of the stream-wise velocity. They are plotted in Fig. 2, where U_J is the nozzle exit mean velocity. A virtual origin x_0 is needed in each of the profiles to collapse the data, although it is very small, indicating that the mixing layer had already achieved a finite thickness at $x = 0$ because of the width

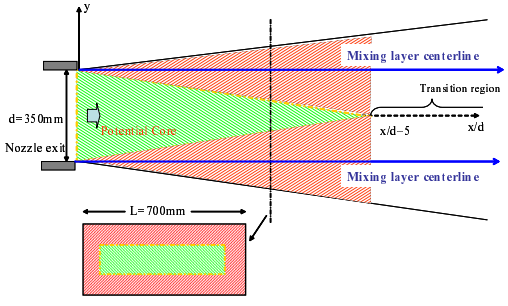

Figure 1: Driving mixing layer and coordinate system.

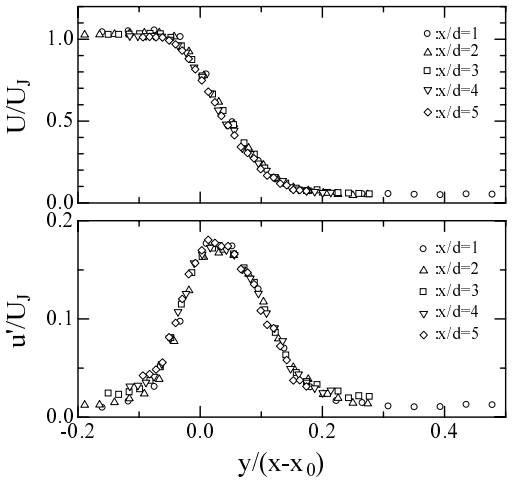

Figure 2: Mean and root mean square of stream-wise velocity component for the case of $U_J = 6.0$m/s. Different symbols indicate different x/d positions.

of the nozzle rip. A simple mean velocity gradient is confirmed in $0 \leq y/(x-x_0) \leq 0.5$, and the normalized intensity u_{rms}/U_J is almost constant. In the following, we analyze the data in this region.

The Taylor-scale Reynolds number; $R_\lambda \equiv u_r\lambda/\nu$, is traditionally used to characterize the turbulence. Here, u_r is the root mean square of stream-wise velocity fluctuation. The Taylor micro scale, λ, is related to the velocity derivative, $\lambda \equiv \sqrt{u_r^2/\left\langle(\partial u/\partial x)^2\right\rangle}$. It does not have a clear physical interpretation, but is a well-defined quantity that is often used. On the other hand, the essential parameter characterizing the shear effect on the small scale is introduced as follows:

$$S^* \equiv (\nu/\langle\varepsilon\rangle)^{1/2} \cdot S \quad , \quad S = dU/dy\,, \tag{1}$$

where $\langle\varepsilon\rangle$ is the energy dissipation rate per unit mass, and S is a mean velocity gradient. The S^* is the ratio of mean shear time scale to the smallest eddy time scale $\tau_\eta \equiv (\nu/\langle\varepsilon\rangle)^{1/2}$, which is called the Kolmogorov time scale. Also the length and velocity scale are defined as $\eta \equiv (\nu^3/\langle\varepsilon\rangle)^{1/4}$ and $u_\eta \equiv (\nu\langle\varepsilon\rangle)^{1/4}$, respectively. If S^* is small, so also the level of anisotropy created by the mean shear might be small. The criterion for the isotropy of the smallest scale is expressed as $S^* \ll 1$. In the simple uniform shear flow, with assuming the energy production equals to the dissipation $\langle\varepsilon\rangle$ and the local isotropy, S^* relates to R_λ as

$$S^* \simeq \frac{1}{a_1}\sqrt{\frac{20}{3}} \cdot R_\lambda^{-1} \propto R_\lambda^{-1}\,, \tag{2}$$

and typical length and velocity scale are simply reduced to

$$L_s = S^{-3/2}\langle\varepsilon\rangle^{1/2} \simeq a_1^{3/2} \cdot L\,, \tag{3}$$

$$u_s = (\langle\varepsilon\rangle/S)^{1/2} \simeq \sqrt{3A_1/2} \cdot u_r\,, \tag{4}$$

where A_1 is Townsend's structure parameter,

$$A_1 \equiv -\langle uv\rangle/\mathbf{u_r} \quad , \quad \mathbf{u_r} = \left[u_r^2 + v_r^2 + w_r^2\right]/2 \tag{5}$$

and $L \equiv \mathbf{u_r}^{3/2}/\langle\varepsilon\rangle$. u_r, v_r, and w_r are root mean square of velocity fluctuation. The relation between S^* and R_λ is plotted in Fig. 3. The data scatter around the relation $S^* \propto R_\lambda$, and we find that this flow field, restricted in the range $0 \leq y/(x-x_0) \leq 0.5$, is close to the simple shear flow.

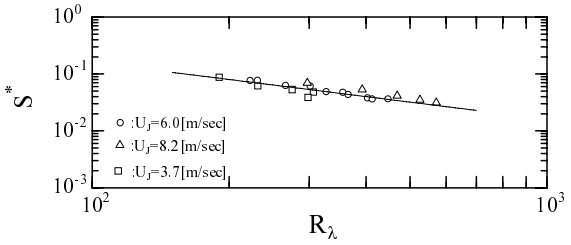

Figure 3: Reynolds number and shear parameter measured in $0 \leq y/(x-x_0) \leq 0.5$. Solid line indicates the relation $R_\lambda \propto S^*$.

Pressure probe and its calibration

The measurement of pressure fluctuation in the flow field is accomplished with a standard 1/8-inch condenser microphone. A microphone is available for measuring the frequency of $10 \sim 70 \times 10^3$Hz. The lower frequency is restricted due to its mechanical system. The dynamic range is $2 \times 10^{-4} \sim 3.2 \times 10^3$ Pa, so a very small amplitude can be measured. The probe is a standard Pitot-static tube measuring $\phi_1 = 0.5$ mm in outside diameter, the tube thickness is $h = 0.05$ mm.

Four static-pressure holes ($\phi_1 = 0.15$ mm in diameter) are spaced 90° apart and located at a distance of $L_1 = 15.5$ mm from the tip of the probe to minimize sensitivity to cross-flow error. The leeward end is terminated by the microphone. The sensor diameters is $d = 2.3$ mm. The detailed sketch is given in the reference (Tsuji et al. 2005).

Yaw angle effect

The pressure sensor is aligned with the probe body axis, which during the experiments in turn is aligned with the mean flow direction implying that a small angle towards the plate is kept. In a preliminary investigation the yaw angle effect, on the measured pressure, between the pressure probe and the mean flow direction was studied. This was done by rotating the probe $-20° \leq \theta \leq +20°$ in the potential core of a round jet, which had an initial velocity of $U_J = 10$ m s^{-1}. For each angle θ the mean differential pressure between the static P_θ and a reference pressure was measured with a manometer (dynamic range 50 Pa), whereupon the corresponding pressure coefficient was calculated according to:

$$C_P = (P_\theta - P_0)\,/\,\frac{1}{2}\rho U_J^2\,. \tag{6}$$

Here, P_0 is the mean pressure at $\theta = 0°$ and in Fig. 4 C_P

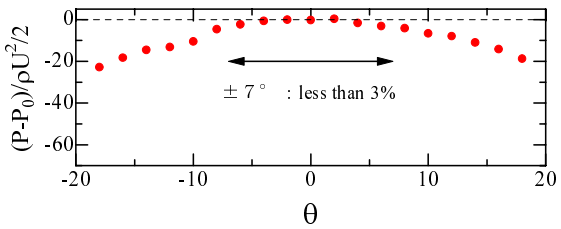

Figure 4: Effect of Yaw angle.

is plotted versus the yaw angle. In the range of $\pm 5°$, we observe $-0.001 < C_P < 0$ and the variation among the different probes is small.

The early analysis of Goldstein (1936) indicated that a static tube reads a pressure equal to $P_m = P + k\rho(v_{rms}^2 + w_{rms}^2)$, where k is a small coefficient. The effect of turbulence on the measured value of static tubes seems to be much smaller than previously known as long as the static tube and pinholes are made small enough (Chue, 1975).

Microphone calibration

When measuring static pressure fluctuations there are not only a direct influence from the probe dimensions chosen, but also an indirect by means of physical flow phenomena that appear inside the probe. Here, this is discussed and the calibration procedure is presented which accounts for all effects by numerical treatment of the static pressure signal.

The calibration of the static pressure probe, operated with the transducer or the microphone as pressure sensor, is done as follows. The probe is set parallel to an opened reference microphone in front of a loudspeaker. A fluctuating pressure stream is generated by a random noise generator and the two signals are acquired simultaneously. The output signal from the pressure probe $p_s(t)$ will not the same as the signal $p_r(t)$ measured by the reference microphone, due to probe influence, Helmholtz resonance, and standing waves. The frequency response of the system is limited by the Helmholtz-resonator (abbreviated as HR) caused by the tube and sensor cavity (Kobashi, 1957; Toyoda, 1993). This HR frequency is calculated as:

$$f_r = \frac{U_s}{2\pi}\sqrt{\frac{S}{L_3 V}}\,, \tag{7}$$

where V is the cavity volume, L_3 is the tube length, U_s is the speed of sound and S is the cross sectional area. For instance, with $V = \pi d^2 L_c/4$ m^3 and $S = \pi(\phi_2)^2/4$ m^2 the resonant frequency is 2.5 kHz and 11.1 kHz for the microphone ($d = 7.0$ mm, $\phi_2 = 1.0$ mm, $L_3 = 18.5$ mm) and the transducer ($d = 1.6$ mm, $\phi_2 = 1.0$ mm, $L_3 = 18.5$ mm), respectively. The amplitude ratio variation and phase delay between the two signals p_s and p_r can be computed by applying the following simple HR model:

$$A_r = \left[\left\{1 - \left(\frac{f}{f_r}\right)^2\right\} + \left(\frac{2\xi f}{f_r}\right)^2\right]^{-1/2}, \tag{8}$$

$$\theta_r = -\tan^{-1}\left\{\frac{2\xi\,(f/f_r)}{1-(f/f_r)^2}\right\}, \tag{9}$$

where ξ is a numerical constant. It should be noted that Eqs. (8) and (9) give an approximation to the measured A_r and θ_r. This model works well if the pressure fluctuation is sufficiently large. But it can be generalized as follows for the smaller pressure intensity.

$$A_r = C_1\left[\left\{1 - \alpha\left(\frac{f}{f_r}\right)^\beta\right\} + \gamma\left(\frac{2\xi f}{f_r}\right)^2\right]^{-1/2}, \tag{10}$$

$$\theta_r = -\tan^{-1}\left\{\frac{2\xi C_2\,(f/f_r)}{1-(f/f_r)^2}\right\}, \tag{11}$$

where α, β, γ, C_1, and C_2 are function of flow condition. In Fig. 5, we indicate how HR changes depending on these parameters. In general, HR is not so significant for small pressure fluctuation. But it becomes large for moderate

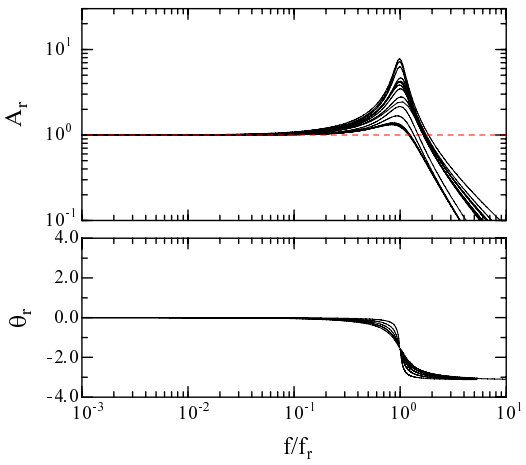

Figure 5: Helmholtz resonance generated inside pressure tube. Amplitude A_r and phase delay θ_r are given in Eqs. (10) and (11).

pressure intensity. In this paper, HR is removed numerically according to the intensity measured in the flow field. Detailed discussions are given in (Tsuji et al., 2007).

A standing wave inside the pressure tube may also cause a small disturbance to the pressure fluctuations. The frequency of the standing wave is given by $f_s = U_s/\lambda_s$ (where $\lambda_s/4 = L_3$), which gives a f_s of about 7.1 kHz for probe1. Another possible limitation may be the spatial resolution of the probe which may be limited by the pinhole size as well as the circumference of the probe itself. For instance, in the log-region at $R_\theta = 16000$ the ratio between the pinhole diameter and the Kolmogorov scale can be estimated to $d/\eta = 1.32$.

In order to achieve accurate measurements, both mean and fluctuations of the measured pressure signal are corrected according to the appropriate calibration. The amplitude ratio and phase delay caused by the HRis removed numerically from the measured signal. Yaw angle effect is negligible in the range of $-5° \le \theta \le 5°$. The standing wave generated inside the tube restricts the time frequency response up to 10 kHz. The spatial resolution is around the Kolmogorov length scale. The background noise is corrected in the statistical sense (this point is not explained here, but see the reference (Tsuji et al., 2007), which can be assumed to be negligible around the centerline in mixing layer.

RESULTS AND DISCUSSIONS

probability density function

Figure 6 shows the static pressure pdfs in the center of mixing layer. Different symbols indicate the different Reynolds numbers and shear parameters. Solid line is the result of nearly isotropic condition (so there is no shear effect). Pdfs are skewed on the negative side and it departs from Gaussian considerably. Around the core, the maximum probability locates a little apart from the centre ($p/\sigma = 0$) to the positive side. It is larger than Gaussian, and the dependence on shear parameter seems to be weak. On the tail parts, negative side deviates from Gaussian significantly, which is decreases as shear parameter decreases. Compared with the case of $R_\lambda = 297$ ($S^* = 0.0695$) with the isotropic

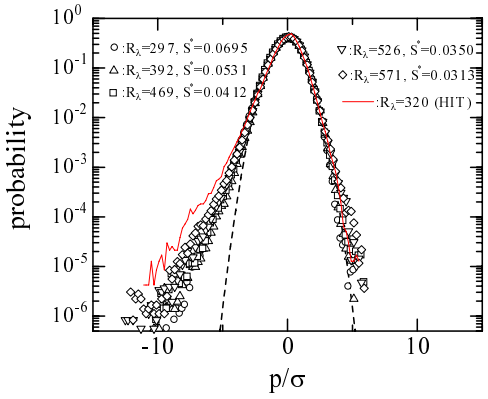

Figure 6: Probability density functions of pressure fluctuations measured in the mixing layer. The solid line is the case of no shear ($dU/dy = 0$).

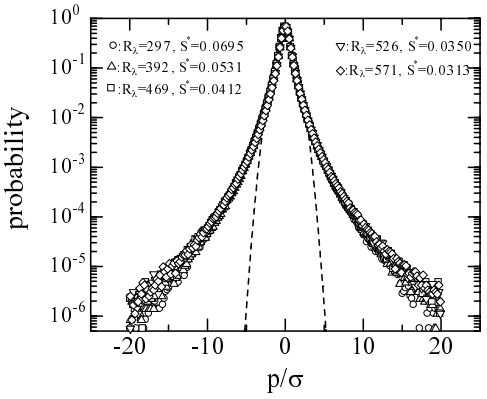

Figure 7: Probability density functions of pressure gradient measured in the mixing layer.

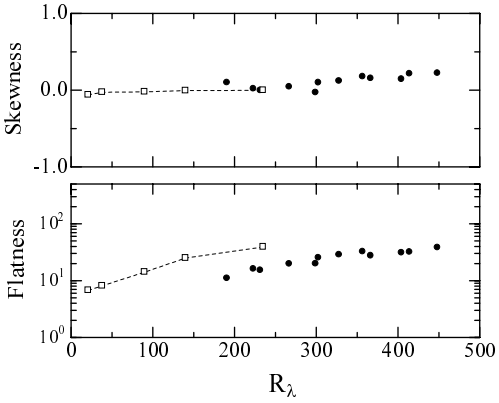

Figure 8: Skewness and flatness of pressure gradient (solid circles). Open square symbols are DNS by Vedula and Yeung (1999).

condition, the positive tail parts are close to Gaussian. However, in the negative tail parts, the mixing layer has a smaller pdf than that of isotropic condition, that is, the shear effect decreases the negative pressure probability. According to the decomposition of p, a mean velocity gradient is included in a source term of rapid pressure $p^{(r)}$, which means that the shear effect appears mainly in $p^{(r)}$. It may be assumed that the negative large-amplitude pressure fluctuation associate with the rapid pressure term.

The pressure difference measured at a distance Δy(or Δx) becomes pressure gradient dp/dy(or dp/dx) as far as Δy (or Δx) is sufficiently small. Here, Δx (or Δy) is set at a few times of Kolmogorov length scale. Pressure gradient distribution has a stretched exponential shape as shown in Fig. 7, in which the tails extend much further than a Gaussian distribution. This indicates that acceleration is an extremely intermittent variable. Different symbols indicate the different Reynolds numbers. As Reynolds number increases, it is found that this intermittency increases. In Fig. 8, the higher order moments are plotted and compared with DNS of homogeneous isotropic condition. The skewness is almost zero and slightly increases in $R_\lambda > 300$. The flatness values in the mixing layer are smaller than DNS results. Thus, we can conclude that the shear effect decrease the intermittent property of pressure gradient. When the flatness of velocity gradient (du/dx, which can be interpreted as Eulerian acceleration) is compared with that of pressure, it is clearly understood that the acceleration field is more intermittent.

spectra

Kolmogorov presented a hypotheses for small-scale statistics based on the idea of local isotropy (Monin and Yaglom,1971), which is restated by the relation,

$$E_{pp}(k_1) = \rho^2 \langle\varepsilon\rangle^{3/4} \nu^{7/4} \phi_p(k_1\eta)\,, \qquad (12)$$

for the one-dimensional energy spectrum of the pressure fluctuations. ϕ_p is a non-dimensional function of the (streamwise) wave number normalized by the Kolmogorov length scale η defined as $\eta = \left(\nu^3/\langle\varepsilon\rangle\right)^{1/4}$, where $\langle\varepsilon\rangle$ is the energy dissipation rate per unit mass on average. According to Kolmogorov's idea, i.e. when the Reynolds number becomes large, the spectrum exhibits an inertial subrange (for $k_1\eta \ll 1$) with a simpler form independent of kinematic viscosity:

$$E_{pp}(k_1) = K_p \rho^2 \langle\varepsilon\rangle^{4/3} \cdot k_1^{-7/3}\,. \qquad (13)$$

The $-7/3$ power-law scaling was supported theoretically with various assumptions in the 1950's by (Batchelor, 1951; Inoue, 1951; Obukhov, 1951). Recently, Tsuji and Ishihara (2003) have examined the pressure spectrum in fully developed turbulence. A power-law exponent of the pressure spectrum was systematically obtained by fitting the relation

$$E_{pp}(k_1) = K_p{}' \rho^2 \langle\varepsilon\rangle^{3/4} \nu^{7/4} (k_1\eta)^{\gamma_p}\,, \qquad (14)$$

against the measured spectra ($K_p{}'$ is a non-dimensional constant quantity). The scaling exponent γ_p was determined by maximizing the width of the spectrum, i.e. which shows the broadest flat region of $E_{pp}/(k_1\eta)^{\gamma_p}$. They measured the static pressure fluctuations on the centreline of a plane turbulent jet for a range of Reynolds numbers ($200 \le R_\lambda \le 1200$), and concluded that if the scaling exponents γ_p are plotted as a function of R_λ, they indeed found a substantial departure from the $-7/3$ value for the exponent at low Reynolds numbers. However they also found the exponent to approach $-7/3$ as the Reynolds number was increased and the $-7/3$ power-law scaling was confirmed for $R_\lambda > 600$. This is a significantly higher Reynolds number than needed for inertial range scaling in velocity statistics. The pressure

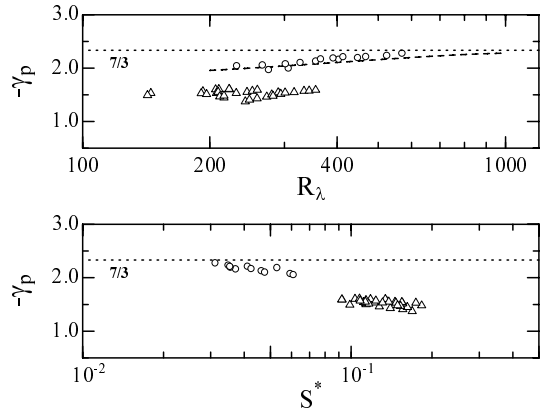

Figure 9: Scaling exponent of pressure spectra defined in Eq.(14) are plotted against Reynolds number and shear parameter.

spectrum has a noticeably narrower scaling region than for the velocity spectrum. This is consistent with the result that a higher Reynolds number is needed to realize a clear $-7/3$ power-law scaling. Not only the Reynolds number but also the shear effect has an important influence on the power-law exponent. In the previous study (Tsuji et al., 2007), we examined the Kolmogorov scaling of pressure fluctuations in the turbulent boundary layer, and evaluated the effect of both shear and Reynolds number on the deviation of γ_p from the $-7/3$ value.

In Figure 9, the exponent γ_p is plotted against the Reynolds number and shear parameter. The results of no shear ($dU/dy = 0$) is plotted as a dashed lined and the values measured in the boundary layer are plotted by symbols. As Reynolds number increases, the exponent approaches to the expected value $-7/3$. In the mixing layer, there is small difference from the case of no shear, but they are much larger than those in boundary layer case. As plotted against the shear parameter, γ_p deviated from the expected value for large S^*. Large shear effect remains in the inertial range, and we assume that the $-7/3$ power-law will be realized in small S^* such as $O(10^{-3})$.

In the acceleration spectra, the expected power-law exponent $-1/3$ is well observed in the present measurements. And the shear effect on the scaling exponent can be discussed in the same way. It is noted that the acceleration spectrum is hard to obtain as far as pursuing the particle trajectories. Following the Kolmogorov's idea, acceleration is scaled by the energy dissipation rate and kinematic viscosity as

$$\langle a_i a_j \rangle = a_0 \varepsilon^{3/2} \nu^{-1/2} \delta_{ij}, \qquad (15)$$

where $a_i = (1/\rho)\partial p/\partial x_i$. The constant a_0 is expected to be universal. But the recent DNS (HIT) and La Porta's experiment do not show that a_0 is not constant but a function of Reynolds number. In a shear flow (Mixing layer), a_0 is much smaller than those of HIT. As R_λ increases, a_0 increases and approaches the values of HIT. Present result indicates that the local isotropy is realized at $R_\lambda \simeq 2000$ in the inertial range. But more detailed discussions are necessary for the shear effect (large scale anisotropy) on the acceleration. This point will be discussed in the presentation.

REFERENCES

S. Ayyalasomayajula, A. Gylfason, L. R. Collins, E. Bodenschatz, and Z. Warhaft, 2006, "Lagrangian Measurements of Inertial Particle Accelerations in Grid Generated Wind Tunnel Turbulence" *Phys. Rev. Letter*, vol. 97, p.144507.

G. K. Batchelor, 1951, "Pressure Fluctuations in Isotropic Turbulence", *Proc. Camb. Phil. Soc.*, vol.47, pp.359–374.

S. H. Chue, 1975, "Pressure Probes for Fluid Measurement", *Prog. Aerospace Sci.*, vol.16, pp.147–223.

S. A. Goldstein, 1936, "A Note on Measurement of Total Head and Static Pressure in a Turbulent Stream", *Proc. Roy. Soc. A*, vol.155, pp.570–575.

W. Heisenberg, 1948, "Zür Statistischen Theorie der Turbulenz", *Z. Phys.*, vol.124, pp.628–657.

J. O. Hinze, 1975," *Turbulence*", McGraw-Hill

E. Inoue, 1951, "The Application of the Turbulence Theory to the Large-Scale Atmospheric Phenomena", *Geophys. Mag.*, vol.23, pp.1–14.

J.S.M.E., 1985,"*JSME Data Book : Flow Measurement*", The Japan Society of Mechanical Engineering, pp.57–60.

Y. Kobashi, 1957, "Measurements of Pressure Fluctuation in the Wake of Cylinder", *J. Physical Soc. Japan*, vol.12, pp.533–543.

A. La Porta and G. A. Voth and A. M. Crawford and J. Alexander and E. Bodenschatz, 2001, "Fluid particle accelerations in fully developed turbulence", *Nature*, vol.409, pp.1017–1019.

M. S. Monin and A. M. Yaglom, 1971, " *Statistical Fluid Mechanics, Vol. 2*", The MIT Press, Cambridge.

A. M. Obukhov, 1949, "Pressure Fluctuations in a Turbulent Flow", *Ddkl. Akad. Nauk SSSR*, vol.66, pp.17–20.

R. Shaw, 1960, "The Influence of Hole Dimensions on Static Pressure Measurements", *J. Fluid Mech.*, vol.9, pp.550–556.

Y. Tsuji and T. Ishihara, 2003, "Similarity Scaling of Pressure Fluctuation in Turbulence", *Phys. Rev. E*, vol.68, p.026309.

Y. Tsuji and J. H. M. Fransson and P. H. Alfredsson and A. V. Johansson", 2005, "Pressure Statistics in High-Reynolds Number Turbulent Boundary Layer", Proc. Fourth Int. Symp. on Turbulence and Shear Flow Phenomena, Williamsburg, VA USA, 27–29 June, Ed. J. A. C. Humphrey and T. B. Gatski and J. K. Eaton and R. Friedrich and N. Kasagi and M. A. Leschziner, pp.27–32. Accepted for publication in Journal of Fluid Mechanics 2007.

K. Toyoda and T. Okamoto and Y. Shirahama, 1993, "Eduction of Vortical Structures by Pressure Measurements in Noncircular Jet", *Fluid Mechanics and its Applications*, vol.21, pp.125–136.

P. Vedula and P. K. Yeung, 1999, "Similarity Scaling of Acceleration and Pressure Statistics in Numerical Simulation of Isotropic Turbulence", *Phys . Fluids*, vol.11, pp.1208–1220.

A. M. Yaglom, 1949, "Acceleration Field in a Turbulent Flow", *Ddkl. Akad. Nauk SSSR*, vol.67, pp.795–798.